

Wave-Tunable Lattice Equivalents toward Micro- and Nanomanipulation

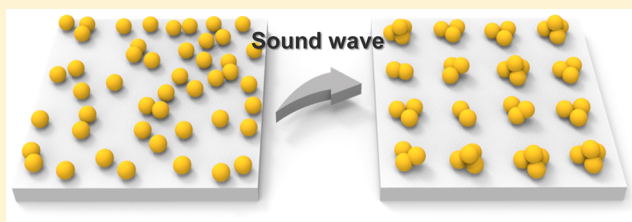
Hyeohn Kim,[†] Taehoon Kim,[†] Dohun Kim,[‡] and Wooyoung Shim^{*,†}

[†]Department of Materials Science and Engineering, Yonsei University, Seoul 120-749, Korea

[‡]Department of Physics and Astronomy, Seoul National University, Seoul 08826, Korea

S Supporting Information

ABSTRACT: The assembly of micro- and nanomaterials is a key issue in the development of potential bottom-up construction of building blocks, but creating periodic arrays of such materials in an efficient and scalable manner still remains challenging. Here, we show that a cymatic assembly approach in which micro- and nanomaterials in a liquid medium that resonate at low-frequency standing waves can be used for the assembly in a spatially periodic and temporally stationary fashion that emerges from the wave displacement antinodes of the standing wave. We also show that employing a two-dimensional liquid, rather than a droplet, with a coffee-ring effect yields a result that exhibits distinct lattice equivalents comprising the materials. The crystallographic parameters, such as the lattice parameters, can be adjusted, where the parameters along the x - and y -axes are controlled by the applied wave frequencies, and the one along z -axis is controlled by a transparent layer as a spacer to create three-dimensional crystal equivalents. This work represents an advancement in assembling micro- and nanomaterials into macroscale architectures on the centimeter-length scale, thus establishing that a standing wave can direct micro- and nanomaterial assembly to mimic plane and space lattices.



KEYWORDS: Sound wave, nanomaterials, bottom-up assembly, coffee ring effect, capillary wave

The crystal lattice is an array of points at which atoms or molecules are positioned that repeats periodically in two or three dimensions and appears exactly the same regardless of the point from which the array is viewed.¹ It describes a highly ordered structure with symmetric patterns characterized by the lengths of the edges of a unit cell, the interaxial angles as lattice parameters, and the symmetry unit represented by the space group. In general, the nature of these lattice parameters that dictate the material properties is not tunable unless it is intentionally engineered, for example, by strain engineering.² Analogous to the situation in a crystal lattice, positioning the materials at a specific point of interest allows one to construct lattice equivalents of different length scales in a way that builds an array of discrete points with an arrangement that has an identical environment around any point. Consistent with this research direction, many efforts have been devoted to the development of nanomaterial alignment and spacing that are tunable on many length scales,^{3–7} leading to the development of integrated functional nanodevices and circuits.⁸ This research has long been motivated by (i) scalable top-down approaches where the particles are assembled in a periodic fashion using mechanical,^{9,10} chemical microcontact printing,¹¹ and parallel scanning probe-based molecular printing^{12,13} and (ii) bottom-up integrated nanomaterial arrays with high registration that are achieved by a variety of forces, such as electric,^{14,15} magnetic,¹⁶ optical,^{17–19} chemical,^{20,21} and mechanical forces.²² In particular, controlling liquid surface tension in a solution²³ has been used for bottom-up assembly of nanowires and carbon

nanotubes, which are potentially scalable and enable the fabrication of large area arrays. Although advances have been made using these solution-based techniques, such as fluid flow²⁴ and the Langmuir–Blodgett technique,²⁵ creating large-area periodic arrays with high registration in an efficient manner remains a challenge. Recently, a nanocombing assembly method that combines attributes of top-down and bottom-up approaches for nanowires was developed, leading to deterministic design large-area logic circuits and nanobioprobe arrays.^{26,27}

In another approach, acoustic energy generated by an ultrasound wave with a frequency in the range from kilohertz to megahertz offers the ability to manipulate microscale-size particles in a fluidic environment.^{28–30} This approach, as it is commonly studied in the area of microfluidics,^{28–32} utilizes the acoustic radiation force associated with a standing ultrasonic wave to trap suspended particles in a host liquid at nodes or antinodes of the wave.^{28–30} For example, the use of the acoustic radiation force in many applications, such as sensing,³¹ collection,³² concentration,³³ and sorting,³⁴ is extensively reported, particularly in a hemispherical droplet where the pattern is limited to a ringlike shape. While taking advantage of the acoustic energy of an ultrasonic wave, this approach does not address the long-standing goal of building periodic lattice

Received: July 18, 2016

Revised: August 20, 2016

Published: August 31, 2016

patterns of nanomaterials that could be also susceptible to damage by high-frequency waves.³⁵ The bottom-up assembly of micro- and nanoscale structures from building blocks such as colloidal spherical particles^{21,36} and anisotropic low-dimensional materials³⁷ is a key challenge, but most research in wave–material interaction has focused on the wave mechanics aspect,^{38,39} leaving our understanding of the assembly of micro- and nanoscale materials at a primitive stage. To realize this goal, a set of rules for using the liquid–material interaction within the wave should be presented in such a way that incorporates the dominant forces that are responsible for the materials assembly and thus deliberately creates a lattice equivalent with wave-dependent size control.

In this paper, we describe a set of rules for achieving micro- and nanomaterial assembly of spatially periodic and temporally stationary patterns in a two- and even three-dimensional fashion that is analogous to a lattice. The lattice is generated in a liquid spread over a square, two-dimensional surface (2D liquid) that resonates to a low-frequency sound wave.^{40–42} Compared to the collection of suspended particles in a liquid droplet, the 2D liquid provides potential advantages in terms of symmetry, sensitivity, and scalability of the pattern. First, in a 2D liquid the position of the node/antinode is highly discrete due to a linear combination of trigonometric functions in Cartesian coordinates, and the projection of the node/antinode is symmetric. Second, because a 2D liquid with low surface energy is highly responsive to wave frequencies there is potential for an aggressive application that requires high sensitivity. Third, because our approach is a method that creates large numbers of arrays in parallel we can create arrays over macroscale areas where the total patterned area is only limited by the size of the plate surface. Below, we first describe the high-symmetry lattice equivalent, which consists of micro- and nanomaterials, and which is highly sensitive to low frequencies at the centimeter scale.

Upon applying a mechanical wave (i.e., a sound wave), randomly distributed particles on a surface can be repositioned, as in the classical Chladni patterns,^{43,44} when the surface vibrates at its resonant frequency. The particles collect at the displacement node or antinode of standing waves such that the particle arrangement can be tuned from an amorphous (statistically homogeneous) to a crystal-like structure (periodically homogeneous) (Figure 1a). This approach addresses the challenge articulated by Hans Jenny in his visionary work,⁴⁵ more than five decades ago, that led to the rise of cymatics: how to observe the vibration phenomena that generate the regular patterns on the resonating surface. In order to explore particle formation systematically, we defined two separate systems (Figure 1b): (i) a spherical coordinate system where the hemispherical droplets are utilized and (ii) a Cartesian coordinate system where liquids on the centimeter-scale plate, which we term 2D liquids in this study, are employed as a medium that can resonate with an applied wave. We formed a droplet with low surface tension, such as ethanol, that contains SiO₂ particles, on a surface of Si. The solution droplet naturally forms part of a hemisphere with a certain contact angle. Upon applying the mechanical wave, standing waves in the form of spherical harmonics determine the position of the nodes and antinodes⁴⁶ (Figure 1b, left) as shown in Supporting Information, S1. On the other hand, by using the 2D liquid on a square substrate, Cartesian coordinates become the more appropriate choice for studying wave dynamics, and for this case we describe the formation of antinodes using trigono-

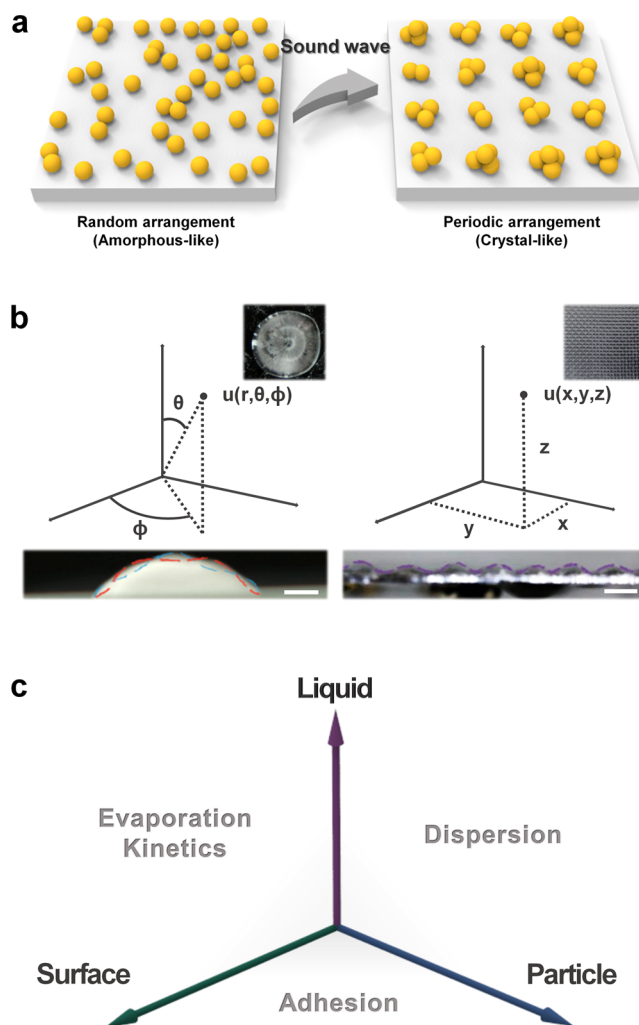


Figure 1. Assembly of micro- and nanomaterials in a fluidic system by applying waves. (a) Micro- and nanomaterials suspended in a liquid medium can be assembled in a periodic fashion by applying waves. (b) A droplet and a two-dimensional liquid of ethanol containing SiO₂ form a ringlike pattern and a grid pattern, respectively, when a vibration of 200 Hz is applied. In hemispherical droplets using the spherical coordination system, the position of nodes and antinodes appear in a concentric pattern (left). The scale bar is 1 mm. In a 2D liquid on a square substrate, described in Cartesian coordinates, the position of the nodal lines forms a two-dimensional grid (right). The scale bar is 5 mm. (c) Three factors contribute to the material assembly. The distribution of particles (liquid–particle interaction) and adhesion (particle–surface interaction) should be considered for material assembly. Furthermore, evaporation kinetics (surface–liquid interaction) have to be considered to pin the particles assembled during the drying process to the substrate.

metric functions⁴⁷ (Figure 1b, right). In both situations, we assume a Neumann boundary condition at the edges of the fluid, which reflects the fact that fluid displacement is zero at the boundaries.

As the scale of materials enters the nano- and microscale regime, the influence of van der Waals interaction between the materials and the surface increases. As a result, the nano- and microscale particles adhere strongly to the surface such that the particles are unlikely to respond to the wave applied to achieve the pattern (Supporting Information, S2). For this reason, a liquid medium was employed as a buffer layer that (i) prevents the strong adhesion of particles to the surface and (ii) readily

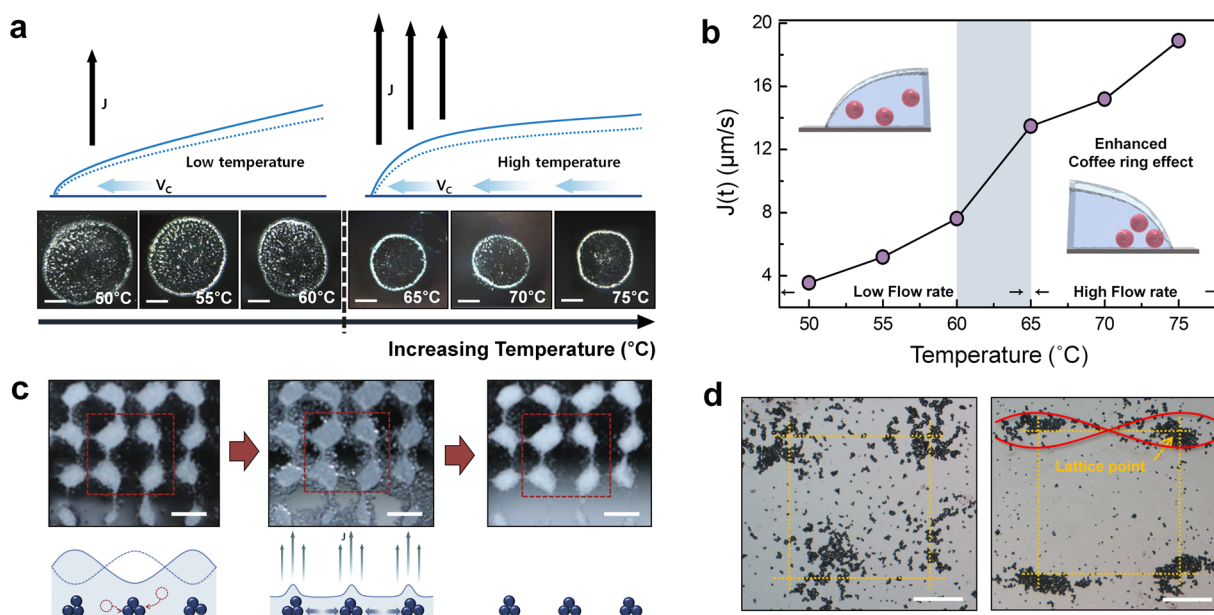


Figure 2. Coffee-ring flow enhancement to achieve particle aggregation. (a) The capillary flow that brings suspended particles to the edge during the evaporation process can be manipulated by the temperature (top). A droplet of ethanol containing SiO_2 microparticles after complete drying at different temperatures from 50 to 75 $^\circ\text{C}$ (bottom). The scale bar is 3 mm. Two different regimes of the particle patterns are plainly distinguishable. A clear ring pattern appeared at high temperatures above T_c (approximately 60 $^\circ\text{C}$). (b) Quantitative analysis of the evaporation rate, $J(t)$ is $Q/A = dV/dt(1/A)$, versus temperature by measurement of the evaporation time and ring pattern areas for a fixed initial droplet volume. A sudden increase in the evaporation rate is observed at T_c (approximately 60 $^\circ\text{C}$). (c) Enlarged photographs (top) and schematic (bottom) of the drying process of the solvent in the 2D liquid. The capillary flow that flows outward from the midpoint is induced during the drying process and particle aggregation is enhanced. The scale bar is 3 mm. (d) Optical microscope (Nikon, Eclipse Ni-E) image of particle aggregation in the 2D liquid after evaporation is completed at room temperature (left) and high temperature above T_c (right). A vibration at 200 Hz was applied to create the particle lattices. The scale bar is 500 μm . Relatively homogeneous dispersion of particles is shown in the lattice points at ambient conditions. On the other hand, the lattice points (particle aggregation) are clearly defined at the high temperature above T_c .

responds to the applied wave in the form of a capillary wave. Qualitatively, several factors contribute to the nano- and microscale material assembly using a nanocymatic approach (Figure 1c). First, the initial distribution of particles (before applying the waves) should be spatially homogeneous, not aggregated with one another in the liquid (Supporting Information, S3). Second, in addition to the size effect mentioned above, hydrophilic particles should be used for hydrophilic surfaces (and vice versa) so that the particles are attracted to the surface (Supporting Information, S4). These two challenges were met in our studies using hydrophilic particles consisting of SiO_2 and a low-surface-energy liquid, ethanol, as the particle and liquid, respectively. In addition, a Si wafer was used as the hydrophilic surface. Third, addressing the vapor–liquid interaction, unlike previous research efforts, which observed particle patterns in the presence of a liquid medium, the particles should aggregate at the displacement antinodes without being dispersed during the drying process of the liquid medium such that the particles remain in place at specific points on the surface. This makes it necessary to study the drying process that enables pinning the particles at specific points as evaporation proceeds, similar to the coffee-ring effect, as described in the paragraph below.

To collect the particles at the antinodes, we utilized the coffee-ring effect in which the particles suspended in a liquid resting on a solid surface leave a ring-shaped structure after the liquid has dried.^{48,49} Specifically, during the drying process the liquid edges become pinned to the surface, and the capillary flow outward from the center of the liquid brings suspended particles to the edge as evaporation proceeds (Figure 2a,

top).^{50,51} Manipulating capillary flows (as indicated by blue arrow in Figure 2a), therefore, is critical to controlling the coffee-ring effect and thus particle collection. Such particle collection that is enhanced by the strong coffee-ring effect leads to a periodic pattern formation. We note that the coffee-ring effect has been observed in several systems with diverse particle sizes and shapes, ranging from anisotropic colloids⁴⁸ to nanoparticles.⁵² This indicates that the coffee-ring effect is not limited to spherical SiO_2 particles but extends to other anisotropic matter such as the Cu nanowire, which will be discussed in the following experiment. The velocity of the liquid moving from the center to the edge of the droplet, v_c , proportional to the magnitude of capillary flow, is determined by the drying process as given by the relationship $v_c = \alpha(Q/A)$, where α is the proportionality constant, Q is the evaporation volume flow rate, and A is the area. This suggests that the capillary flow can be readily enhanced by increasing v_c through an increase in the evaporation volume flow rate Q , where $Q = dV/dt$ and V is the evaporated volume and t is the evaporation time. Therefore, our strategy is to increase dV/dt , which can be simply controlled by the temperature as indicated by the relationship $v_c(t, T) = \alpha(dV(t, T)/dt)(1/A)$. Initially, as a proof-of-concept for the application of temperature control in enhancing the coffee-ring effect, our experiments used an ethanol drop containing a suspension of SiO_2 particles (of approximately 50 μm diameter). Briefly, to prepare the droplets the SiO_2 particles were homogeneously dispersed in ethanol and then the drops with an average area $A = 59.9 \text{ mm}^2$ and volume $V = 10 \mu\text{L}$ were placed on the Si surface and heated to temperatures ranging from 50 to 75 $^\circ\text{C}$. After completely

drying, images of the SiO₂ particles on the Si surface were made to indicate the temperature effect (Figure 2a, bottom). Interestingly, at a constant relative humidity and particle concentration, we observed two distinct regimes for the particle deposits that appeared above or below a critical temperature, T_c . The first regime appears when the droplets dried at temperatures below T_c , where the suspended particles are dispersed homogeneously. In the second regime, the particles are efficiently transported to the edge of the drop when drying takes place above T_c . Taken together, these results confirm that high drying temperatures are crucial to increasing the capillary flow that in turn increases the coffee-ring effect and thus meets the requirements for particle positioning outlined schematically in Figure 1c. To the best of our knowledge, a quantitative analysis of a drying ethanol droplet with suspended particles has not been reported.

To quantify the drying process shown qualitatively in Figure 2a, we determined the evaporation rate of the liquid, $J(t)$, which is proportional to the magnitude of capillary flow as given by the relationship $J(t) = Q/A = dV/dt(1/A) \sim (V/t)(1/A)$ (Figure 2b).⁵³ We assumed that the particle motion in the liquid does not affect the evaporation process, and a capillary flow from the center of drop to the edge replenishes fluid at the contact line as the evaporation proceeds. In fact, it was found that there was a transition temperature range. Below T_c (approximately 60 °C), where the particles were dispersed homogeneously, the values of J were found to be 4 (50 °C), 6 (55 °C), and 8 $\mu\text{m/s}$ (60 °C), while above T_c the values of J were 13 (65 °C), 16 (70 °C), and 19 $\mu\text{m/s}$ (75 °C). In general, as the temperature increases, the cohesive energy (between liquid molecules) decreases, whereas the adhesion energy (between the liquid molecules and the atoms of the solid surface) increases.^{54,55} The contact angle of the liquid droplet, therefore, decreases and, as a consequence, larger dried edges form. In contrast, based on our observations the size of the dried edges above T_c was found to decrease as shown in Figure 2a. Specifically, a 57% reduction of area, A , compared to the dried edges at temperatures below T_c was observed, leading to the sudden increase in $J(t)$, as shown in Figure 2b. These results can be understood by considering a rapid evaporation rate, which is faster than the rate of increase in adhesion energy as the temperatures increase, especially for the low-boiling-point solvent ethanol. Note that this method holds for a wide range of particle diameters (Supporting Information, S5), and it can therefore be used to increase the coffee-ring effect with increased capillary flow, enabling particle aggregation.

Whereas increasing the capillary flow in the droplets by increasing the temperature offers a dramatic demonstration of particle aggregation at the droplet edges, increasing the capillary flow in the liquid on a surface in a two-dimensional Cartesian system provides a powerful platform for studying the particle aggregation over a large area. Indeed, one could envision an experiment in which the particles collect at the displacement antinode when a standing wave is applied to the liquid, and the liquid evaporates causing the particles to settle in a particular position. As in the case of the droplets where particle aggregation is enhanced by increasing capillary flow, we envision that the particle aggregation in the 2D liquid can be achieved by increasing the evaporation rate (by enhancing the coffee-ring effect). In the text below, we describe the capillary flow in the 2D liquid and then demonstrate the particle aggregation after evaporation is complete.

First, we investigated how the particles in the 2D liquid collect at the displacement antinodes of standing waves. As in Figure 1a, the particles were collected at the specific points where the displacement antinodes appear as a grid-like pattern (Figure 2c, left), as opposed to the ring-like patterns resulting from the liquid droplet (Figure 2a). In general, the fluid moves vertically at the displacement antinode, while it moves horizontally around the node (no vertical displacement), which is responsible for the movement of the particles to the displacement antinode. At low frequencies (<1 kHz), as in our study, hydrodynamic focusing was the mechanism by which the particles responded to the vibrating fluid motion and moved to the antinode, similar to the acoustic radiation force mechanism at high frequencies (>100 kHz).⁵⁶ Second, we characterized how the concept of capillary flow in the liquid droplet can be applied to the capillary flow in the 2D liquid, namely, the coffee-ring effect at the multiple points in the liquid where the particles are collected at the antinode. We carried out continuous observation using an optical microscope and readily demonstrated that capillary flow is responsible for collecting particles at the antinodes. Similar to the line created by pinned particles that resulted from the liquid droplet, we found that the points where the particles collected kept, or pinned, the liquid in place during evaporation and, as a result, induced capillary flow that flowed outward from the midpoint, where the particles were not positioned (Figure 2c, middle). The experiments thus demonstrate that despite different contact line (or point) forms between the circular (droplet) and 2D Cartesian systems, the evaporation rate and capillary flow significantly affect the particle aggregation in the coffee-ring effect (Figure 2c, right). To support this point, we also carried out an experiment (at frequency $f = 200$ Hz) where the 2D liquid evaporates at ambient conditions (i.e., room temperature); these measurements show the relatively homogeneous dispersion of the particles (amorphous) after evaporation is complete (Figure 2d, left). Conversely, the particle aggregation, which we term the lattice that occurs after evaporation at a temperature above T_c is complete, is fairly well-defined (crystal-like) as a function of dV/dt (Figure 2d, right). A clear coffee-ring effect strengthened by capillary flow persists for a high evaporation rate ($T > T_c$), but a low evaporation rate ($T < T_c$) leads to uniform dispersion of the particles. Notably, for the first time this work describes the realization of the coffee-ring effect in the 2D liquid, which is unlikely to be obtained at ambient conditions because of low capillary flow.

Through a cymatic approach (Supporting Information, S6 and S7), lattices with periodic symmetry can be created from diverse wave frequencies; square arrays were created by applying sound wave frequencies of 50, 100, 200, 300, and 400 Hz (Figure 3a). There is an inverse relationship between the resonant frequencies and wavelength given by $f = v/\lambda$, where v is the speed of the traveling wave in the liquid and λ is the wavelength. The distance between particle lattices (between antinodes), analogous to $\lambda/2$, can be varied with the applied f in that it decreases as the frequency increases as schematically shown in the insets of Figure 3a. To interpret these lattices, we developed an indexing system based on the reciprocal lattice generated by a discrete Fourier transform of a two-dimensional real space lattice of optical images using the relation $I_{k_x, k_y} = \sum_{n_x, n_y=0}^{N-1} i_{n_x, n_y} e^{-(2\pi i k_x n_x + 2\pi i k_y n_y)/N}$, where I_{k_x, k_y} is the discretized Fourier transform of the real-space intensity i_{n_x, n_y} at pixel n_x and n_y and N is the image size represented in pixels.

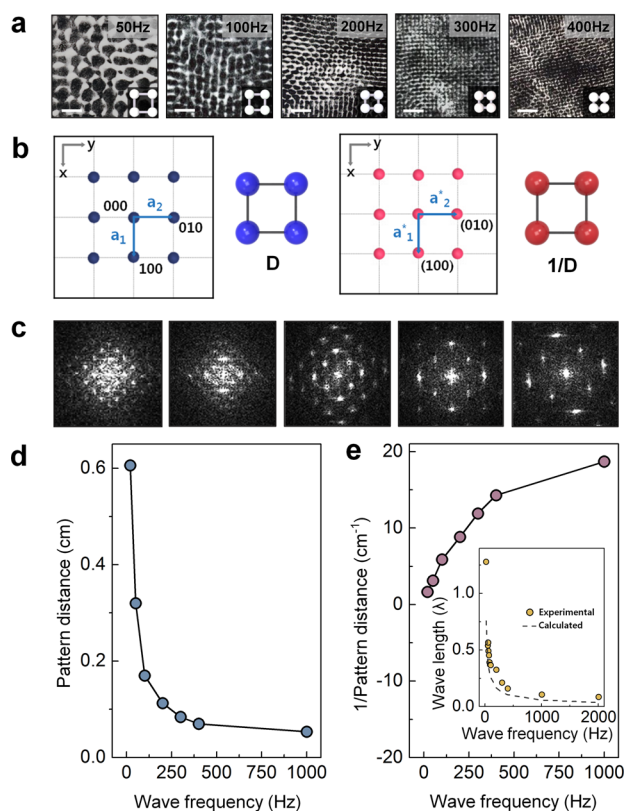


Figure 3. Square arrays of microparticles generated by the capillary waves on the surface of the liquid medium. (a) Lattices with square arrays of SiO_2 microparticles created by applying sound wave frequencies of 50, 100, 200, 300, and 400 Hz. The scale bar is 5 mm. As the frequency increases, more nodes and antinodes are generated. As shown in the insets of Figure 3a, the pattern distance becomes smaller as the frequency increases. (b) Indexing system of a real space lattice and a reciprocal lattice generated by a Fourier transform. Each point (hkl) in the reciprocal space corresponds to a plane (hkl) in the real space. The magnitude of the reciprocal lattice distance is equal to the inverse value of the interplanar spacing in the real space. (c) Computer-generated images obtained by the Fourier-transform of the square dot arrays in panel a. Reciprocal lattices with dot arrays without continuous ring arrays show the periodicity of square dot lattices in panel a. The distance between dots in the reciprocal lattices increases as the distance between points in the real lattices decreases. (d) Graph showing the distance between lattices in real space for frequencies from 50 Hz to 1 kHz. As the frequencies increase, the lattice distances, d_{100} (or d_{010}), decrease. (e) Distance between the reciprocal lattices for frequencies from 50 Hz to 1 kHz. The distance between the reciprocal lattices, d^*_{100} (or d^*_{010}), is linearly proportional to the applied frequencies. Particle lattices are formed by the capillary waves in the medium. The capillary waves carry particles to the antinodes of the standing waves. A comparison of the experimental and calculated capillary wavelength versus frequency plots shows very good agreement in the inset of panel e.

For the automated Fourier transform calculation, we used National Instruments Vision Development Module 8.5 along with the LabVIEW development platform. In general, the construction of a reciprocal lattice from the corresponding direct lattice is performed as follows: for each set of lattice planes (hkl) , the normal is drawn from the origin with a length $d^*_{hkl} = 1/d_{hkl}$ where d is the lattice spacing. For example, the normal to the set of lattice planes (100) is drawn from the origin and assigned a length $d^*_{100} = 1/d_{100}$ and a point a^*_1 , and a similar construction for the set of (010) planes gives the point

a^*_2 with a length d^*_{010} (Figure 3b). The points a^*_1 and a^*_2 represent the relative orientations of the (100) and (010) planes. The use of the reciprocal lattice allows a discussion of the application of Fourier transform patterns as shown in Figure 3c: the Fourier transform of the particle patterns shows square dot arrays (bright spots) without continuous ring arrays, which represents the regular periodicity of the square patterned lattices. In addition, the distance between dots in the reciprocal lattices, analogous to d^*_{hkl} , increased as d_{hkl} decreased (Figure 3c). From the quantitative perspective, as the frequencies increase in the range from 50 Hz to 1 kHz, the lattice distances, d_{100} (or d_{010}), decrease from 3.2 mm to 530 μm (Figure 3d). In addition, the distance between the lattices in the reciprocal lattice, d^*_{100} (or d^*_{010}), is linearly proportional to the applied frequencies (Figure 3e) and therefore verifies an inverse relationship with d_{100} (or d_{010}) (Supporting Information, S8). These dynamics, which are qualitatively identical to those of standing waves with the given frequencies in the medium, account for the mechanism in which the particle lattices are formed by and placed at the antinodes of the applied waves. In addition, comparison of the wavelength versus frequency of the experimental and the calculated capillary wave,^{57,58} defined by $\omega^2 \lambda^3 = 2\pi\gamma/\rho$, where ω is the frequency, γ is the surface tension of the liquid medium, and ρ is the density, shows excellent agreement (inset of Figure 3e). This agreement substantiates the existence of a capillary wave that carries the particles to the antinodes in these experiments (Supporting Information, S9).

Having demonstrated that this approach can yield defined lattice patterns, we explore the potential for this technique to generate a wider range of lattices. First, a high degree of precision in the placement of particles can be seen in the reciprocal lattices of the Fourier transform (Figure 4a). Interestingly, even with small intervals of 5 Hz, the distinct d^*_{100} for each experiment can be achieved with frequencies ranging from 50 to 150 Hz (Figure 4b). To quantify d^*_{100} , we count the number of pixels between the origin and a^*_1 in the Fourier transform images (346×346 pixels per image). The linear correlation between the number of pixels and frequencies ensures that a capillary wave in the liquid with low surface tension (20 mN/m), rather than the resonance of the surface material, is generated by the applied wave and thus maximizes the particle aggregation and pattern formation. This level of sensitivity is substantially higher than in other previous reports and is hardly, if ever, achievable even for the patterns driven by ultrasonic wave frequencies. The ability to control the precise pattern distance and size, and in particular increase the sensitivity by utilizing capillary flow in the 2D liquid, is distinct from previous studies where the analytical interpretations were not available. This technique can provide flexibility for realizing complex patterns with the materials of interest.

To verify the general applicability of this new strategy in constructing lattice equivalents of more complex structures, we built three-dimensional lattice structures by controlling the size of a_3 along the z -axis. Specifically, SiO_2 particles were first patterned on the glass surface, followed by the deposition of a transparent polymer layer (i.e., polydimethylsiloxane, PDMS) that served as another surface for the following SiO_2 particle pattern. An oxygen-plasma treatment (100 W, 30 s, 500 mTorr) was used to induce the hydrophilicity of the PDMS surface. Because the capillary flow in the liquid is responsible for positioning the particles, constructing the lattice equivalents is not dependent on the type of surface. In establishing the lattice parameters, we assumed that the thickness of the

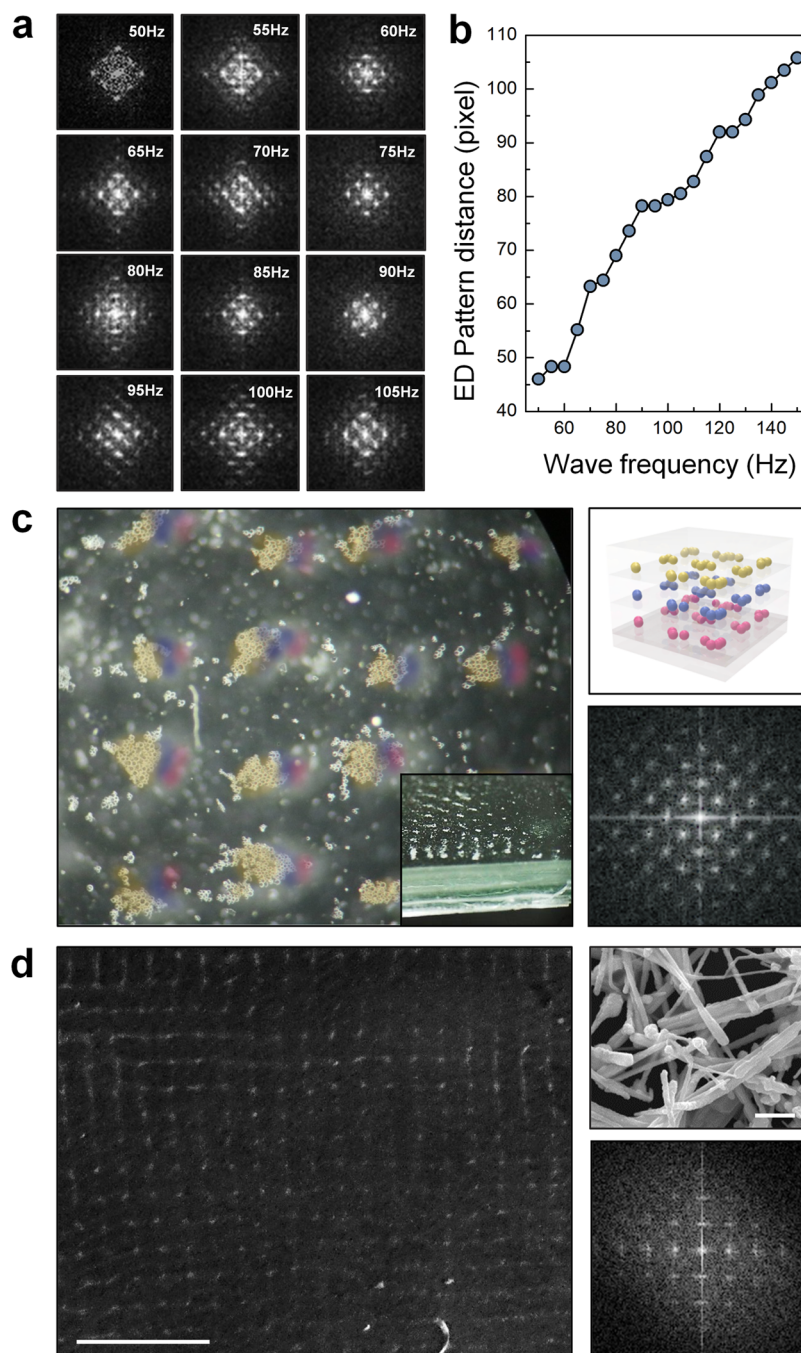


Figure 4. Three-dimensional lattice equivalents and nanowire assembly with a high degree of precision. (a) Fourier transforms of lattices of SiO_2 microparticles at frequencies from 50 to 105 Hz at 5 Hz intervals. Reciprocal lattices with square dot arrays are shown. (b) To quantify the distances between reciprocal lattices, the number of pixels between the lattices is counted. The number of pixels in the Fourier transform images is 346×346 pixels per image. The placement of the particles shows a high degree of precision even at the small intervals of 5 Hz. The capillary waves in the liquid medium with a low surface tension maximize the level of sensitivity of the particle patterning. (c) Three-dimensional lattice structures with SiO_2 microparticles created by controlling the size of a_3 along the z -axis. Three layers of two-dimensional lattices are overlapped between the transparent spacers. The insert image was taken while the sample was tilted at an angle of $\sim 70^\circ$. The lattice points formed on the three surfaces overlap because the capillary flow in the liquid is not dependent on the type of surface. Reciprocal lattices (bottom right) confirm the regular periodicity of the three-dimensional lattice equivalents. (d) Assembly of nanowires, tens of nanometers in diameter and $\sim 5 \mu\text{m}$ in length, using the same experimental procedures as for particles. An optical photograph (left) and an SEM (JEOL JSM-7001F) image (top right) of a particle lattice equivalent of copper nanowires. The scale bar of the optical image is 5 mm (inset, 500 μm) and of the SEM image is 5 μm . The nanowires show excellent assembly at the lattice point with a lattice distance of ~ 1 mm. Reciprocal lattices (bottom right) also confirm the regular periodicity of the nanowire assembly.

polymer layer determines a_3 along the z -axis. In addition, the precise pattern control allows one to position particles on the PDMS at lattice points identical to those of the prepatterned lattices on the Si surface and therefore the interaxial angle γ

(between the z - and x - y planes) is 90° . The optical microscope image (Figure 4c) unequivocally shows the high degree of order in the created superlattice, where a_1 is equal to a_2 , but not to a_3 ($a_1 = a_2 \neq a_3$) as in a tetragonal crystal system. Note that

the inset image was taken while the sample was tilted intentionally (by an angle of $\sim 70^\circ$) for imaging purposes. The reciprocal lattices also confirmed that the lattices are in regular periodicity, and the lattice points formed on both surfaces are spatially overlapped (a_1 at 100 = a_1 at 101).

Last, we demonstrate a general method for constructing a lattice equivalent to achieve a nanowire assembly. The assembly of nanowire, tens of nanometers in diameter and approximately 5 μm in length, represents a significant challenge for the development of a range of bottom-up devices but has the potential to enable nanodevice integration. Using the same experimental procedures as described above for the copper nanowires demonstrates excellent aggregation at the lattice points (or displacement antinodes of the capillary wave) with an average lattice distance of approximately 1 mm (Figure 4d). Indeed, the assembly done by nanowire aggregation (top-right image of Figure 4d) is clearly observed at the lattice points where $a_1 = a_2$, and its lattice points are also in periodicity on the centimeter scale (bottom-right image of Figure 4d). Interestingly, this level of nanowire assembly is to the best of our knowledge the first demonstration using wave-driven methods and greatly facilitates an assembly strategy without any pretreatment chemistry or external electric and magnetic fields.

We have developed a new assembly strategy whereby 2D liquids subject to low-frequency standing waves are kinetically controlled to enable orderly positioning of micro- and nanomaterials with distinct symmetry in patterns that are difficult to obtain and in some cases have not previously been observed in the context of 3D lattices. Although most studies of wave-induced particle distribution to date have focused on understanding the fundamental principles of wave mechanics and visualizing waves by observing particles on liquid surfaces, the use of low frequency waves applied to 2D liquids simply constructs a lattice of assembled particles, rather than disks or rings of particles from a droplet. Furthermore, our method is the first to use a spacer layer made of a transparent polymer to create 3D lattices of particles. We have also shown that the coffee-ring effect in particle assembly is readily applicable to other particle types, and the system is highly sensitive to the applied wave frequencies. This method does have disadvantages compared to previous researches. For example, it is less suitable to be used for fabrication of single nanomaterial-based nanodevices because the lattice equivalents in this study lack well-defined local nanoscale structures. This limitation includes (i) local concentration in which the density of nanomaterials at each lattice point is not highly controllable and thus is not monodisperse; (ii) local symmetry in which the nanomaterial aligned show less directional control, that is, for nanowires; (iii) local registration in which positioning of each lattice point with precise location in nanometer scale is further needed to be improved. We also note that the method is currently limited to micro- and millimeter scales in the context of the pattern distance, but this issue may be addressed by exploring the viscosity of liquid subject to high frequency standing wave to decrease the pattern distance and, as a consequence, increase the pattern density. The additional structural diversity will be useful in the development of nanomaterial alignment and assembly and will be needed to fully exploit the new capabilities afforded by this method.

Methods. *Fabrication of 2D Lattices with Microparticles.* SiO_2 microparticles with a diameter of approximately 50 μm and a bulk density of 1.52 kg/L were suspended in ethanol. A silicon wafer (iTASCO) was cut into a square shape (4 cm \times 4

cm) with a diamond pencil for use as a substrate. Using carbon tape, the silicon substrate was attached to a wave driver (PASCO, SF-9324) in a horizontal position. Then, the solution containing the microparticles was dropped on the substrate. Vertical vibrations of the wave driver were induced by a function generator (PASCO, PI-8127) at diverse frequencies from 20 to 1000 Hz until an array of patterns was generated. To minimize fluctuation in the liquid, the vibration was slowly stopped by reducing the voltage applied by the function generator. To augment the evaporation of the solvent, the substrate was heated with an infrared heating device (ZAIGLE, ZGSimple) after the wave driver operation had stopped. The substrate remained fixed to the wave driver until the solvent was completely evaporated, and it was removed from the wave driver.

Construction of a Three-Dimensional Lattice Equivalent. A piece of square-shaped soda lime glass (5 cm \times 5 cm) was used as a substrate for the three-dimensional lattice equivalent. The substrate was exposed to oxygen plasma (100 W, 30 s, 500 mTorr) to reduce the hydrophobicity of the soda-lime glass surface. Using the method described above, a 2D-lattice pattern of SiO_2 microparticles was fabricated on the substrate using a 200 Hz frequency. After using the oxygen plasma on the substrate to achieve strong adhesion between the substrate and a PDMS spacer, a 10:1 mixture of PDMS elastomer (Dow Corning, Sylgard 184) was vacuum-degassed and poured onto the substrate to a thickness of 750 μm . The PDMS spacer layer was cured on a hot plate at 90 $^\circ\text{C}$ for 90 min. A 2D lattice pattern of SiO_2 microparticles was fabricated on the oxygen-plasma-treated PDMS surface using the same frequency of 200 Hz. A three-dimensional lattice equivalent was constructed by repeating the same process.

■ ASSOCIATED CONTENT

📄 Supporting Information

The Supporting Information is available free of charge on the ACS Publications website at DOI: 10.1021/acs.nanolett.6b02973.

Additional figures (PDF)

■ AUTHOR INFORMATION

Corresponding Author

*E-mail: wshim@yonsei.ac.kr.

Notes

The authors declare no competing financial interest.

■ ACKNOWLEDGMENTS

This research was supported by Basic Science Research Program through the National Research Foundation of Korea (NRF) funded by the Ministry of Science, ICT & Future Planning (2014K2A1A2048494), the National Research Foundation of Korea (NRF) Grant funded by the Korean Government (MSIP) (2015R1A5A1037668), the Priority Research Centers Program (2009-0093823), the Small Grant for Exploratory Research (S GER) (NRF-2014R1A1A2A16055867), and Korea Sanhak Foundation (2014).

■ REFERENCES

(1) Smith, W. F.; Hashemi, J. *Foundations of Materials Science and Engineering*, 5th ed.; McGraw-Hill: New York, 2011; p 84.

- (2) Deshpande, S.; Patil, S.; Kuchibhatla, S. V.; Seal, S. *Appl. Phys. Lett.* **2005**, *87*, 133113.
- (3) Yu, G.; Lieber, C. M. *Pure Appl. Chem.* **2010**, *82*, 2295–2314.
- (4) Lu, W.; Lieber, C. M. *J. Phys. D: Appl. Phys.* **2006**, *39*, R387–R406.
- (5) Whang, D.; Jin, S.; Wu, Y.; Lieber, C. M. *Nano Lett.* **2003**, *3*, 1255–1259.
- (6) Pevzner, A.; Engel, Y.; Elnathan, R.; Ducobni, T.; Ben-Ishai, M.; Reddy, K.; Shpaisman, N.; Tsukernik, A.; Oksman, M.; Patolsky, F. *Nano Lett.* **2010**, *10*, 1202–1208.
- (7) Liu, J.; Xie, C.; Dai, X.; Jin, L.; Zhou, W.; Lieber, C. M. *Proc. Natl. Acad. Sci. U. S. A.* **2013**, *110*, 6694–6699.
- (8) Lu, W.; Lieber, C. M. *Nat. Mater.* **2007**, *6*, 841–850.
- (9) Santhanam, V.; Andres, R. P. *Nano Lett.* **2004**, *4*, 41–44.
- (10) Cucinotta, F.; Popović, Z.; Weiss, E.; Whitesides, G. M.; Cola, L. D. *Adv. Mater.* **2009**, *21*, 1142–1145.
- (11) Kraus, T.; Malaquin, L.; Schmid, H.; Riess, W.; Spencer, N. D.; Wolf, H. *Nat. Nanotechnol.* **2007**, *2*, 570–576.
- (12) Chen, P. C.; Liu, X.; Hedrick, J. L.; Xie, Z.; Wang, S.; Lin, Q. Y.; Hersam, M. C.; Dravid, V. P.; Mirkin, C. A. *Science* **2016**, *352*, 1565–1569.
- (13) Chai, J.; Huo, F.; Zheng, Z.; Giam, L. R.; Shim, W.; Mirkin, C. A. *Proc. Natl. Acad. Sci. U. S. A.* **2010**, *107*, 20202–20206.
- (14) Duan, X.; Huang, Y.; Cui, Y.; Wang, J.; Lieber, C. M. *Nature* **2001**, *409*, 66–69.
- (15) Freer, E. M.; Grachev, O.; Duan, X.; Martin, S.; Stumbo, D. P. *Nat. Nanotechnol.* **2010**, *5*, 525–530.
- (16) Hangarter, C. M.; Myung, N. V. *Chem. Mater.* **2005**, *17*, 1320–1324.
- (17) Pauzaskie, P. J.; Radenovic, A.; Trepagnier, E.; Shroff, H.; Yang, P.; Liphardt, J. *Nat. Mater.* **2006**, *5*, 97–101.
- (18) Agarwal, R.; Ladavac, K.; Roichman, Y.; Yu, G.; Lieber, C. M.; Grier, D. G. *Opt. Express* **2005**, *13*, 8906–8912.
- (19) Gates, B. D.; Xu, Q.; Stewart, M.; Ryan, D.; Willson, C. G.; Whitesides, G. M. *Chem. Rev.* **2005**, *105*, 1171–1196.
- (20) Rao, S. G.; Huang, L.; Setyawan, W.; Hong, S. *Nature* **2003**, *425*, 36–37.
- (21) Macfarlane, R. J.; Lee, B.; Jones, M. R.; Harris, N.; Schatz, G. C.; Mirkin, C. A. *Science* **2011**, *334*, 204–208.
- (22) Javey, A.; Nam, S. W.; Friedman, R. S.; Yan, H.; Lieber, C. M. *Nano Lett.* **2007**, *7*, 773–777.
- (23) Yu, G.; Cao, A.; Lieber, C. M. *Nat. Nanotechnol.* **2007**, *2*, 372–377.
- (24) Huang, Y.; Duan, X.; Wei, Q.; Lieber, C. M. *Science* **2001**, *291*, 630–633.
- (25) Tao, A.; Kim, F.; Hess, C.; Goldberger, J.; He, R.; Sun, Y.; Xia, Y.; Yang, P. *Nano Lett.* **2003**, *3*, 1229–1233.
- (26) Zhao, Y.; Yao, J.; Xu, L.; Mankin, M.; Zhu, Y.; Wu, H.; Mai, L.; Zhang, Q.; Lieber, C. M. *Nano Lett.* **2016**, *16*, 2644–2650.
- (27) Yao, J.; Yan, H.; Lieber, C. M. *Nat. Nanotechnol.* **2013**, *8*, 329–335.
- (28) Rogers, P.; Gralinski, I.; Galtry, C.; Neild, A. *Microfluid. Nanofluid.* **2013**, *14*, 469–477.
- (29) Johansson, L.; Enlund, J.; Johansson, S.; Katardjiev, I.; Yantchev, V. *Biomed. Microdevices* **2012**, *14*, 279–289.
- (30) Oberti, S.; Neild, A.; Quach, R.; Dual, J. *Ultrasonics* **2009**, *49*, 47–52.
- (31) Glynne-Jones, P.; Boltryk, R. J.; Hill, M.; Zhang, F.; Dong, L.; Wilkinson, J. S.; Melvin, T.; Harris, N. R.; Brown, T. *Anal. Sci.* **2009**, *25*, 285–291.
- (32) Hultström, J.; Manneberg, O.; Dopf, K.; Hertz, H. M.; Brismar, H.; Wiklund, M. *Ultrasound Med. Biol.* **2007**, *33*, 145–151.
- (33) Hill, M.; Shen, Y.; Hawkes, J. J. *Ultrasonics* **2002**, *40*, 385–392.
- (34) Petersson, F.; Nilsson, A.; Holm, C.; Jönsson, H.; Laurell, T. *Lab Chip* **2005**, *5*, 20–22.
- (35) Huang, Y. Y.; Knowles, T. P. J.; Terentjev, E. M. *Adv. Mater.* **2009**, *21*, 3945–3948.
- (36) Yin, Y.; Xia, Y. *Adv. Mater.* **2001**, *13*, 267–271.
- (37) Li, M.; Bhiladvala, R. B.; Morrow, T. J.; Sioss, J. A.; Lew, K.; Redwing, J. M.; Keating, C. D.; Mayer, T. S. *Nat. Nanotechnol.* **2008**, *3*, 88–92.
- (38) Gedge, M.; Hill, M. *Lab Chip* **2012**, *12*, 2998–3007.
- (39) Tan, M. K.; Friend, J. R.; Matar, O. K.; Yeo, L. Y. *Phys. Fluids* **2010**, *22*, 112112.
- (40) Christiansen, B.; Alström, P.; Levinsen, M. T. *Phys. Rev. Lett.* **1992**, *68*, 2157–2160.
- (41) Falkovich, G.; Weinberg, A.; Denissenko, P.; Lukaschuk, S. *Nature* **2005**, *435*, 1045–1046.
- (42) Denissenko, P.; Falkovich, G.; Lukaschuk, S. *Phys. Rev. Lett.* **2006**, *97*, 244501.
- (43) Rossing, T. D.; Fletcher, N. H. *Principles of Vibration and Sound*; Springer Science+Business Media New York, Inc.: New York, 2004; pp 65–88.
- (44) Oh, Y. J.; Kim, S. *Ijet* **2012**, *4*, 434–436.
- (45) Jenny, H. *Cymatics*; Macromedia, Inc.: New York, 2001.
- (46) Kreyszig, E. *Advanced Engineering Mathematics*, 10th ed.; John Wiley & Sons, Inc.: New York, 2011; pp 593–597.
- (47) Kreyszig, E. *Advanced Engineering Mathematics*, 10th ed.; John Wiley & Sons, Inc.: New York, 2011; pp 582–583.
- (48) Yunker, P. J.; Still, T.; Lohr, M. A.; Yodh, A. G. *Nature* **2011**, *476*, 308–311.
- (49) Deegan, R. D.; Bakajin, O.; Dupont, T. F.; Huber, G.; Nagel, S. R.; Witten, T. A. *Nature* **1997**, *389*, 827–829.
- (50) Shen, X.; Ho, C.; Wong, T. J. *Phys. Chem. B* **2010**, *114*, 5269–5274.
- (51) Popov, Y. O. *Phys. Rev. E* **2005**, *71*, 036313.
- (52) Bigioni, T. P.; Lin, X.; Nguyen, T. T.; Corwin, E. I.; Witten, T. A.; Jaeger, H. M. *Nat. Mater.* **2006**, *5*, 265–270.
- (53) Bazargan, V. Effect of substrate cooling and droplet shape and composition on the droplet evaporation and the deposition of particles. Unpublished Ph.D. Dissertation, Department of Mechanical Engineering, University of British Columbia, 2014; p 83.
- (54) Podesta, M. D. *Understanding the Properties of Matter*; Taylor & Francis Inc.: New York, 2002; p 295.
- (55) Yamamoto, M.; Nakajima, K. *Wear* **1981**, *70*, 321–327.
- (56) Whitehill, J.; Neild, A.; Ng, T. W.; Stokes, M. *Appl. Phys. Lett.* **2010**, *96*, 053501.
- (57) Kenyon, K. E. *J. Oceanogr.* **1998**, *54*, 343–346.
- (58) MacDowell, L. G.; Benet, J.; Katcho, N. A.; Palanco, J. M. G. *Adv. Colloid Interface Sci.* **2014**, *206*, 150–171.